Title: Asymmetric dispersal is a critical element of concordance between biophysical dispersal models and spatial genetic structure in Great Barrier Reef corals

Authors: Cynthia Riginos, Karlo Hock, Ambrocio M. A. Matias, Peter J. Mumby, Madeleine J. H. van Oppen, Vimoksalehi Lukoschek

Affiliations:
CR: School of Biological Sciences, The University of Queensland, St Lucia QLD, Australia; c.riginos@uq.edu.au
KH: School of Biological Sciences, The University of Queensland, St Lucia QLD, Australia; k.hock1@uq.edu.au
AMAM: School of Biological Sciences, The University of Queensland, St Lucia QLD, Australia; ambrocio.matias@uqconnect.edu.au
PJM: School of Biological Sciences, The University of Queensland, St Lucia QLD, Australia; p.j.mumby@uq.edu.au
MJHvO: School of BioSciences, The University of Melbourne, VIC 3010, Australia; Australian Institute for Marine Sciences, Cape Cleveland QLD 4810, Australia; madeleine.van@unimelb.edu.au
VL: ARC Centre of Excellence for Coral Reef Studies, James Cook University, Townsville QLD 4811, Australia; vimoksalehi.lukoschek@jcu.edu.au

Authorship statement: CR, VL, and KH conceived the study. KH created the biophysical dispersal models, AMAM undertook the coalescent analyses, and CR conducted all remaining analyses and figure preparations. VL and MLHvO provided the data. CR wrote the first draft of the manuscript, and all authors contributed substantially to revisions.

Data accessibility statement: Raw data available at datadryad.org/resource/doi:10.5061/dryad.h8gh3 for *Acropora tenuis* and datadryad.org/resource/doi:10.5061/dryad.q0834p71 for *Acropora millepora.*

Running title: Asymmetric dispersal in GBR corals

Key words: Approximate Bayesian Computation, asymmetric eigenvector modelling, connectivity, gene flow, marine landscape, Moran eigenvector modelling, oceanography, planktonic dispersal, seascape genetics

Correspondence: School of Biological Sciences, University of Queensland, St Lucia QLD, Australia; c.riginos@uq.edu.au, +61 7 336 52152

Abstract

Documenting and predicting spatial connections arising from planktonic larval dispersal in marine species remains a formidable challenge. Biophysical dispersal models using simulations based on biological attributes and physical oceanography are attractive predictive tools. Here we evaluate how such simulated long-distance multigenerational connections align with spatial genetic data for two common coral species (*Acropora tenuis* and *Acropora millepora*) from the Great Barrier Reef (GBR), Australia. We focus on signatures of asymmetric dispersal and evaluate concordance using coalescent genetic simulations, directions of inferred gene flow, and spatial eigenvector modelling. The strongest matches rely on asymmetric north to south connections, consistent with biophysical dispersal models yielding approximate summaries of past multigenerational gene flow conditioned upon directionality. For *A. tenuis* and *A. millepora,* northern and central reefs have been important sources to downstream southern reefs over the recent evolutionary past, yet endemic diversity of southern reefs also suggests substantial recruitment of local progeny.

Introduction

Understanding the spatial dynamics of dispersal by planktonic marine larvae remains a fundamental challenge in marine ecology (Carr *et al.* 2003; Kritzer & Sale 2004). Currents and other oceanographic phenomena are inherently dynamic such that dispersal-mediated connections among populations are difficult to predict and vary by time and place (Cowen & Sponaugle 2009; Watson *et al.* 2012; Liggins *et al.* 2013; Gaggiotti 2017). Yet, knowledge regarding the sources and destinations of dispersive larvae underpin fundamental ecological and evolutionary dynamics and inform optimal management of marine resources for fishing and the protection of key habitats (Beger *et al.* 2010; Gaines *et al.* 2010; Hock *et al.* 2017; Krueck *et al.* 2017).

Coupled biological-physical models (Werner & Cowen 2007; Cowen & Sponaugle 2009) relying on simulations based on species attributes and physical oceanography are increasingly being used to predict spatial and temporal aspects of planktonic larval dispersal. The flexibility of both spatio-temporal scale and outputs makes biophysical models extremely well-suited for alignment against various sources of empirical dispersal data (Cowen & Sponaugle 2009; Kool *et al.* 2013; Liggins *et al.* 2013; Jones 2015) and for generating detailed spatial predictions useful for management assessments (as in Hock *et al.* 2016; 2017; Krueck *et al.* 2017).

The extent to which biophysical models accurately approximate real dispersal phenomena, however, remains an open question. As models of open natural systems, strict validation or rejection of biophysical dispersal models is not feasible (Oreskes *et al.* 1994). Rather, such models can be evaluated against empirical data whereby alignment of the model and empirical data confers increased confidence that both the model and empirically-derived statistics describe the phenomenon of interest, in this case dispersal of planktonic larvae. Geographic surveys of intraspecific genetic variation can provide important insights regarding dispersal (Hellberg 2009; Riginos & Liggins 2013; Selkoe *et al.* 2016a) and indeed several studies have considered predictions arising from biophysical dispersal models alongside observed spatial genetic patterns, typically for coastal marine taxa. Although some individual studies report correlations (Galindo *et al.* 2006; White *et al.* 2010; Schunter *et al.* 2011; Foster *et al.* 2012; Thomas *et al.* 2015; Benestan *et al.* 2016; Truelove *et al.* 2016; Dalongeville *et al.* 2018; Xuereb *et al.* 2018), a recent review of the field found only moderate

77 to low concordance between biophysical predictions and empirical genetic patterns (Selkoe *et*
78 *al.* 2016b).
79
80 There are many reasons why biophysical dispersal models and genetic data may not align.
81 First, biophysical models typically focus solely on dispersal and do not consider differential
82 recruitment and/or reproductive success of settlers (Pineda *et al.* 2007). Second, a
83 biophysical model might not sufficiently account for important biological attributes of larvae
84 or complex near shore oceanography, which are notoriously difficult to parameterise (Pineda
85 *et al.* 2007; Werner & Cowen 2007; Metaxas & Saunders 2009). Third, there is a mismatch in
86 time scales, where biophysical models draw upon oceanographic information collected within
87 recent years or decades whereas genetic inferences, especially those based on population
88 allele frequency differences, arise from long term processes (thousands of years and longer).
89 Fourth, population allele frequencies do not solely reflect gene flow resulting from dispersal
90 but are also shaped by changes in population sizes, range expansions, colonization and so
91 forth (Whitlock & McCauley 1999). Lastly, although biophysical models typically predict
92 asymmetric directionality of dispersal, typical descriptors of genetic diversity are symmetric
93 so that statistical comparisons between biophysical models and empirical genetic data nearly
94 exclusively rely on transforming modelled dispersal predictions into symmetric measures,
95 greatly reducing the information content (Kool *et al.* 2013; Riginos *et al.* 2016).
96
97 Only a few studies have attempted to ascertain whether empirical genetic patterns are
98 specifically consistent with the asymmetric dispersal processes inherent to biophysically
99 derived dispersal predictions. For example, migration matrices derived from biophysical
100 modelling were used to inform gene flow in forward population genetic simulations (Galindo
101 *et al.* 2006) and to analytically predict genetic differentiation based on forward matrix
102 projections (Kool *et al.* 2010; 2011), yielding outcomes that qualitatively matched empirical
103 genetic patterns. For the Caribbean coral *Orbicellea annularis*, genetic distances derived from
104 a forward matrix project were shown to be well correlated ($\rho = 0.49$) to empirical genetic
105 distance estimates (Foster *et al.* 2012). Another strategy draws upon historical demographic
106 simulations to quantify migration values consistent with empirically observed allele
107 frequency spectra or DNA sequences. For example, Matz *et al.* (2018) documented correlation
108 between population pairwise estimates of migration derived from allele frequency spectra
109 against biophysically derived migration probabilities for five populations for the coral

110 *Acropora millepora* from the Great Barrier Reef (GBR) (Mantel R = 0.58, P = 0.05), with a
111 preponderance of southward migration consistent between both measures. Comparing all
112 sampled populations holistically, Crandall *et al.* (2012) constructed a series of coalescent
113 models of gene flow and contrasted the likelihood of observed DNA haplotype distributions
114 from the biophysically-informed gene flow models against various other null geographic
115 models; they demonstrated greater likelihood of biophysically informed gene flow models
116 across three species of nerite snails in the South Pacific. Recently, three studies turned to
117 asymmetric eigenvector mapping (AEM: Blanchet *et al.* 2011) where asymmetric processes
118 (such as biophysical migration probabilities) are statistically modelled as spatial
119 autocorrelation structures; inclusion of AEMs substantially improved predictions of spatial
120 genetic structure for American lobster (Benestan *et al.* 2016), California sea cucumbers
121 (Xuereb *et al.* 2018), and Mediterranean striped red mullet (Dalongeville *et al.* 2018). Thus,
122 these first few studies that quantitatively incorporate asymmetric biophysical predictions
123 suggest that directions of larval dispersal are important elements of marine population
124 connectivity.
125
126 Here, we comprehensively assess the alignment between biophysical models of dispersal and
127 observed spatial genetic patterns for two common broadcast spawning coral species on the
128 GBR, *Acropora tenuis* and *Acropora millepora*, drawing upon methods based on historical
129 demographic simulations, patterns of shared alleles, and AEM spatial autocorrelation
130 structures. We capitalise upon spatially rich genetic data sets for the two species (van Oppen
131 *et al.* 2011; Lukoschek *et al.* 2016) with sampling encompassing most of the 2300 km extent
132 of the GBR. Oceanographic patterns suggest that directional gene flow is likely for GBR species
133 such as *A. tenuis* and *A. millepora* (Fig. 1a).
134
135 Although present-day oceanography implies that larval dispersal can create connections
136 among distant reefs, several species show differentiation between central/northern vs.
137 southern GBR locations (reviewed by van Oppen *et al.* 2011), indicative of possible historical
138 vicariance associated with past sea level changes. This divergence is most notable for the
139 spiny chromis damselfish for which genetically distinct colour morphs abut at the north end
140 of Hydrographer's Channel (Planes & Doherty 1997). Recent geological investigations,
141 however, have identified reef structures along the Australian shelf edge that may have
142 provided coral reef habitat during intermediate and low sea level stands (Abbey *et al.* 2011;

143 Hinestrosa *et al.* 2016), implying that reef species may have shifted their range margins
144 through multiple glacial cycles following the depth contours of available coastline but
145 maintaining their approximate latitudinal positions.
146
147 No single method can simultaneously infer modern and historical gene flow regimes across
148 numerous sites spanning large spatial scales. Rather than discounting historical influences (as
149 is implicit in many spatial genetic studies), we use coalescent demographic simulations to
150 evaluate competing scenarios of long-standing gene flow vs. late Quaternary divergence. The
151 resultant affirmation of gene flow-dominated demography along the GBR justifies subsequent
152 frequentist analyses focusing on directional gene flow inferred from population allele
153 frequencies and using all sampled reefs. Treating the biophysical models as hypotheses of
154 spatial connections among GBR reefs for *Acropora* corals, we test whether projected
155 asymmetric directions and dispersal strengths are superior predictors of spatial genetic
156 patterns as compared to simple symmetric null predictors. In addition, we examine the spatial
157 scales and regions for which biophysical predictors best align to observed genetic patterns.
158 This study provides a framework for aligning spatially rich population genetic data against *a*
159 *priori* predictions of asymmetric dispersal and represents the most comprehensive analysis of
160 asymmetric gene flow along the full length of the GBR to date.
161
162 **MATERIAL AND METHODS**
163 *Multi-step connectivity pathways based on larval dispersal models*
164 Dispersal simulations follow Hock *et al.* (in review) and are described in the supplementary
165 materials. The resultant region-wide species-specific connectivity networks (incorporating all
166 3806 GBR reefs) were used to predict multistep paths between the reefs from which the
167 genetic samples were obtained. To calculate the minimum number of *stepping-stones* between
168 two reefs in a connectivity network, all the positive link weights were set to 1. Links in this
169 unweighted network include connections that were present at least once over the four years
170 of simulations regardless of the strength of connection. Dijkstra's (1959) algorithm yielded
171 the directed path with the minimum number of stepping-stones between any two reefs.
172 *Maximum flow* metric calculations were performed by applying a maximum-flow minimum-
173 cut algorithm (Ford & Fulkerson 1956) on a weighted connectivity network in which link
174 weights were considered to represent flow capacities. Determining the capacities of links
175 necessary to connect the two nodes in a network (including multistep paths) then makes it

176 possible to determine the maximum amount of flow between them. The maximum flow metric
177 was calculated using the Matlab implementation of Boykov-Kolmogorov max-flow algorithm
178 (Boykov & Kolmogorov 2004). It is also possible to consider that link weights represent
179 probabilities of dispersal (i.e., the probability that larvae from reef *i* will disperse to reef *j*), by
180 multiplying the link probabilities on pathways connecting two reefs, with the most *reliable*
181 *path* representing the greatest chance of exchange (applying Dijkstra's algorithm to the
182 network using negatively log-transformed link weights - see Hock & Mumby 2015).
183
184 *Genetic data*
185 We capitalise on the extensive microsatellite datasets for *Acropora tenuis* (Lukoschek *et al.*
186 2016) and *Acropora millepora* (van Oppen *et al.* 2011). These data were filtered to remove
187 identical multilocus genotypes and individuals or loci with excessive missing data. Loci were
188 checked for confirmation to Hardy-Weinberg proportions and an absence of linkage
189 disequilibria. See supplementary materials for full details. For *A. tenuis*, we retained 1928
190 individuals from 39 sites genotyped at 10 loci and for *A. millepora*, we retained 917
191 individuals from 19 sites genotyped at 10 loci.
192
193 *Resolving historical influences using coalescent-based ABC*
194 If allele frequencies among *Acropora* populations have been strongly influenced by past
195 interruptions to gene flow, then we would need to evaluate observed geographic
196 differentiation in light of such a divergence history. In contrast, if gene flow has dominated the
197 modern distributions of allelic diversity then dispersal interpretations based on observed
198 allele frequencies are reasonable. We used an approximate Bayesian computation (ABC)
199 approach to test the competing hypotheses of historical divergence vs. stepping-stone gene
200 flow, with the location of historical divergence set at the northern opening of Hydrographer's
201 Passage (Fig. 1). Owing to the high computational requirement in simulating genetic data for
202 our full datasets, we used representative populations for our ABC analyses (Figure S1). A
203 custom R script drew parameter values from the prior distributions, which were used with
204 fastSimcoal2 v2.6.0.3 (Excoffier *et al.* 2013) to generate a total of 500,000 simulations of ten
205 microsatellite loci for each genetic model. The simulated genetic data were summarised using
206 the following statistics calculated with the Arlequin command-line version arlsumstat v3.5.2.2
207 (Excoffier & Lischer 2010): average number of alleles, standard deviation of number of alleles,
208 allele size range per population, and average pairwise F_{ST} between populations. We limited

209 the summary statistics to these measures to avoid extreme high dimensionality of summary
210 statistics while retaining pertinent information about genetic diversity in each population and
211 genetic differentiation between populations.
212
213 In determining the support for each genetic model (model selection), we first obtained
214 posterior samples from all the simulated data for each species by applying a threshold of 0.01,
215 equivalent to the 10,000 simulated datasets closest to the observed genetic data. We then
216 evaluated the support for each genetic model by performing a categorical regression
217 (Beaumont 2008) on the model indices and summary statistics of the posterior samples.
218 Model cross validation was undertaken on pseudo-observed data (PODs). See supplementary
219 materials for further details.
220
221 *Asymmetric gene flow and larval dispersal connectivity*
222 To estimate directionality of gene flow we use information from semi private alleles between
223 pairs of populations (Sundqvist *et al.* 2016) as implemented by divMigrateOnline
224 (https://popgen.shinyapps.io/divMigrate-online/) using the G_{ST} option (with no threshold for
225 filtering out non-significant values). We assessed the correlation between these asymmetric
226 (directional) estimates of gene flow with asymmetric measures of connectivity derived from
227 the larval dispersal model (described above). Significances of the correlations were evaluated
228 using 10,000 permutations. Maximum flow and reliable path metrics were (natural) log
229 transformed for these and subsequent evaluations.
230
231 *Spatial eigenvector mapping*
232 Although isolation-by-distance approaches have long been applied in spatial genetic contexts,
233 they fail to account for spatial autocorrelation structures. Moran Eigenvector Maps (MEMs)
234 model orthogonal spatial structures and, when combined with multivariate analyses, can test
235 for spatial regression (Borcard & Legendre 2002; Dray *et al.* 2006) and are well-suited for
236 genetic investigations (Diniz-Filho *et al.* 2009). Asymmetric eigenvector maps (AEMs) extend
237 spatial modelling to describe spatial structures arising from directional processes such as
238 ocean currents (Blanchet *et al.* 2008; 2011). Here we use AEMs derived from the biophysical
239 model to test whether asymmetric (directional) connectivity distances predict genetic
240 structure, with AEM model fits contrasted to null symmetric expectations described by MEMs.
241

242 For (symmetrical) MEMs, we followed Dray *et al.* (2006) and examined binary Delauney,
243 weighted Delauney, and truncated (principal coordinates of neighbour matrices: PCNM)
244 networks based on spatial position (i.e. geographic distance between sites) with a variety of
245 link weighting schemes to alter the relative influence of short vs. long distance connections
246 (see Supp.). A custom saturated network allowing connections among combinations of sites
247 was also used as an analogue to conventional isolation-by-distance analyses.
248
249 The construction of AEMs requires specifying connexion diagrams (Blanchet *et al.* 2008;
250 2011) indicating directionality of predicted process (in this case larval dispersal). Initial
251 examination of connections for both species indicated a preponderance of strong connections
252 (Fig. 1) southwards alongshore and westward cross-shelf (approximately NE to SW)
253 especially connecting the Swains to Keppel Island and to the Capricorn-Bunker group. Several
254 northwards alongshore connections were also predicted especially from outer shelf to central
255 reefs. For AEMs, we constructed a series of connexion diagrams summarising the main
256 system-wide connection directions (see Fig. 1), allowing north to south alongshore
257 connections with an inshore bend in the southern GBR connecting the Swains to the
258 Capricorn-Bunker group and Keppels. We also created connexion diagrams for south to north.
259 In each case, models were fit with north to south only and in both directions. Connection links
260 were created for all population pairs with reliable path probabilities in the top 50th percentile.
261 Link weightings based on the number of stepping stone connections, maximum flow, and
262 reliable path were evaluated. For *A. tenuis* where special coverage was more extensive, we
263 also fit AEMs to adjacent sets of regions (far north and north; north, central and south; central
264 and south).
265
266 **RESULTS**
267 *Larval dispersal model*
268 Larval dispersal models for *Acropora tenuis* and *Acropora millepora* suggest that GBR
269 populations are well connected when multi-step (i.e. multigenerational) connections are
270 considered. Overall southward connections were more prevalent, especially long-distance
271 connections: this can be visualised by vectored arcs curving the right in Fig. 1B and C along
272 with greater dispersal probabilities for southwards movements (Fig. 1 D and E). However,
273 some strong northward connections were also present (vectored arcs curving the left)
274 especially among central reefs and some central to northern reefs. All three multistep

275 connectivity metrics considered were highly correlated ($\rho \geq 0.86$ for *A. tenuis*; $\rho \geq 0.82$ for *A.*
276 *millepora*) with the greatest correlations between stepping stone distance and reliable paths
277 ($\rho \geq 0.99$ for both species). Given these high correlations, we present results primarily for the
278 reliable path metric, which arguably best aligns with biological intuitions regarding
279 population connectivity across time (Hock & Mumby 2015).
280
281 *Resolving historical influences using coalescent-based ABC*
282 In the present study it was necessary to verify that gene flow has shaped *Acropora* spatial
283 genetic patterns and exclude vicariance as an alternative scenario before proceeding with
284 analyses that implicitly ignore divergence. Indeed, ABC analyses yielded higher support for
285 the gene flow only stepping-stone model (*A. tenuis*: PP= 0.999; BF = 1210; *A. millepora*: pp=
286 0.647; BF = 3) compared to a model of historical divergence vicariance. Applying model
287 selection with the PODs yielded high accuracy (> 99%; proportion of PODs that were correctly
288 supported) and high robustness (> 99% with thresholds above 0.6 PP). Overall, these results
289 indicate strong support (*sensu* Roux *et al.* 2016) for the gene flow only stepping-stone model
290 for both species.
291
292 *Asymmetric gene flow and larval dispersal connectivity*
293 For *A. tenuis*, all directional predictors of connectivity yielded significant correlations with
294 relative gene flow estimates from divMigrate (ρ values for stepping stone distance: -0.39;
295 maximum flow: 0.32; reliable path: 0.37; in all cases $P << 0.001$). For *A. millepora*, reliable
296 path ($\rho = 0.16$; $P < 0.005$) and stepping stone distances ($\rho = - 0.13$; $P < 0.03$) were significantly
297 correlated with relative gene flow but maximum flow was not ($\rho = 0.06$; NS).
298 For both species, inspecting the relationship between reliable path probabilities and gene
299 flow (Fig. 2) shows that for populations predicted to be well connected by the larval dispersal
300 model (i.e. $P \geq 10^{-20}$) estimates of relative gene flow were highly variable (~0-1), whereas
301 sites predicted to require many stepping stone connections ($P \leq 10^{-40}$) had consistently lower
302 gene flow estimates. This pattern was stronger in *A. tenuis* than *A. millepora*.
303
304 *Spatial eigenvector mapping*
305 Directional spatial autocorrelation as assessed by AEMs explained a greater proportion of
306 variance in allele frequencies for both species (Table 1), where the best models were based on
307 alongshore north to south movements with inshore connections from the Swains to Keppel

308 Island and to the Capricorn-Bunker group (for *A. tenuis*, R^2 = 0.37 with 9 AEMs retained and
309 for *A. millepora*, R^2 = 0.27 with 5 AEMs retained). There was no consistency in terms of best-
310 performing link weighting (i.e. stepping stone connections, maximum flow, and reliable path)
311 and notably the binary weighting (presence vs. absence, no weighting by distance) for north
312 to south connections in *A. millepora* was the best performing, indicating that simply
313 recognising strong connections (i.e. those with reliable path probabilities in the top 50th
314 percentile) yields good approximations of spatial genetic patterns. Fig. 3 depicts the highest
315 scoring AEMs for *A. tenuis* where AEM 1 (3.5% of allele frequency variance; P = 0.001) as the
316 largest scale of positive autocorrelation showed a gradient across the entire sampled region of
317 the GBR and AEM 5 (2.3% of variance; P = 0.001) described more local scale autocorrelation
318 patterns. For *A. tenuis*, AEMs 1, 5, 17, 3, 2, and 12 were individually significant at a P = 0.05
319 threshold based on an RDA of the final model where higher numbers (i.e. AEM17) indicate
320 finer spatial grain sizes out of a total of 19 possible AEMs of positive spatial autocorrelation.
321 Similar results were found for *A. millepora* (Supp Fig. 5) with AEM 1 describing the greatest
322 amount of spatial variance in allele frequencies (5.9%, P = 0.003) followed by AEM 8 (5.7%, P
323 = 0.007), and AEMs 1, 8, 5, and 3 individually significant below a P = 0.05 threshold out of 9
324 AEMs evaluated. For *A. tenuis*, sampling within regions was sufficiently dense to evaluate fits
325 for adjacent regions of competing AEM models. In all instances links based on north to south
326 alongshore flow returned the best scoring models, with fit to allelic frequency patterns
327 notably lower in the far northern and northern reefs (Table 2).
328
329 **DISCUSSION**
330 Asymmetric dispersal is undoubtedly a common attribute of benthic marine species. For the
331 corals *Acropora tenuis* and *Acropora millepora*, a preponderance of north to south movement
332 along the GBR was predicted by biophysical models and this directional signal was matched in
333 patterns of microsatellite allele frequencies. Although previous studies have noted distinct
334 characteristics of northern + central vs. southern + Swains + Capricorn-Bunker regions (van
335 Oppen *et al.* 2011; Lukoschek *et al.* 2016), here we can confirm asymmetric gene flow as a
336 contributor to these regional differences. Alternative scenarios involving historical divergence
337 and symmetric gene flow were poor matches to observed spatial genetic patterns relative to
338 scenarios based on directions and extent of larval exchange predicted by biophysical models.
339 Thus, at least at the regional scale within the GBR, oceanography is likely to strongly influence
340 connections arising from planktonic larval dispersal.

341

342 *Regional connections among GBR populations*

343 Whereas geographically restricted alleles are a hallmark of long-standing isolation, highly
344 directional dispersal such as among coastal populations can result in regionally private alleles
345 in downstream populations if dispersal is sufficiently rare and when accompanied by high
346 self-recruitment of settlers to their parental populations (Pringle & Wares 2007). This
347 expectation qualitatively matched diversity gradients for both *Acropora* species (as noted by
348 Lukoschek *et al.* 2016). Here, coalescent demographic simulations allowed us to formally
349 evaluate a hypothesis of Quaternary divergence against a scenario of long-standing gene flow
350 without divergence. For *A. tenuis,* we found very high support for gene flow without
351 divergence (posterior probability: 0.999; BF = 1210) and moderate support for this scenario
352 in *A. millepora* (PP= 0.647; BF = 3). Thus, if there were past divergence events, the imprint of
353 such events is no longer discernible from extant allele frequencies and present-day
354 population genetic structure should be strongly influenced by recent gene flow.

355

356 Indeed, contemporary biophysical expectations for gene flow, were strong predictors of
357 genetic patterns especially at large spatial scales. Using shared alleles, the weakest genetically
358 connected population pairs (negligible gene flow from reef *i* to reef *j*) match pairs having the
359 weakest predicted multigenerational connection links (Fig. 2). Where the biophysical
360 dispersal models predicted stronger connections, in contrast, inferred gene flow was highly
361 variable indicating that at shorter distances the biophysical models and gene flow were not
362 consistently aligned. Formal statistical testing for spatial structure of allelic distributions with
363 MEMs and AEMs reinforced these findings, where eigenvectors derived from predicted
364 asymmetric connections explained considerably more variance than eigenvectors derived
365 from null geographic models of symmetric connections (Table 1). Additionally, for both *A.*
366 *tenuis* and *A. millepora* AEM 1, which describes the largest scale pattern of spatial
367 relationships (Fig. 3 and Sup. Fig. 2), explained the greatest proportion of variance in allelic
368 distributions (3.5 and 5.9%, respectively). AEM analyses, however, were also consistent with
369 spatial patterning at smaller spatial scales arising from asymmetric connections (Table 1).

370

371 Although spatial distributions of microsatellite alleles for both *A. tenuis* and *A. millepora* were
372 broadly consistent with asymmetric dispersal predicted by biophysical models, the best
373 alignments were obtained only considering the approximately north to south connections

374 along the length of the GBR (Table 1). Notably biophysical models for both species suggested
375 substantial counterflows (south to north) especially among inshore reefs (Fig. 1), yet adding
376 these connections to AEM models did not increase model fit (Table 1). Thus, either the
377 stronger north to south connections are sufficient for capturing most of the microsatellite
378 allelic variance or the predicted south to north movements are not realised: for example,
379 larvae may conceivably disperse northwards but could have low fitness and therefore not
380 make substantive contributions to gene flow. Matz *et al.* (2018) also detected greater
381 southwards migration among five populations of GBR *A. millepora* based on ~11,500
382 nucleotide polymorphisms, albeit with some northwards migration. Southward spread also
383 characterises Crown-of-Thorns starfish outbreaks that appear to originate in northern reefs
384 (Pratchett *et al.* 2014). Therefore, our finding of a strong southward dispersal signal is
385 compatible with these other results, but the sensitivity of AEM based analyses to bidirectional
386 flows is unclear.
387
388 For *A. tenuis* we were able to further assess correlations between biophysical predictions and
389 allelic spatial distributions between adjacent regions (Table 2). For southern and central
390 reefs, north to south connections models yielded the best fits to the data ($R^2 \geq 0.32$). These
391 observations spatially align with major jets from the Coral Sea encountering the GBR and
392 driving southward advective flows along the GBR (i.e. surface waters of the South Caledonia
393 Jet at the top of the central region and Eastern Australian Current at the Swains: Choukroun *et*
394 *al.* 2010; Mao & Luick 2014). In contrast, far northern and northern reefs showed reduced
395 concordance between predictions and genetic observations ($R^2 = 0.17$) with a model based on
396 bidirectional connections yielding the best fit to this regional data; surface waters of the North
397 Caledonia Jet encounters the GBR here and creates both northward and southward flows and
398 thus might explain a possible signal of bidirectional connections among *A. tenuis* populations
399 (Choukroun *et al.* 2010; Mao & Luick 2014). For both species, biophysical models predict rare
400 dispersal connections especially among far northern reefs (Fig. 1) and yet negligible
401 population structure was observed for either *A. tenuis* or *A. millepora* among reefs in the far
402 north (Lukoschek *et al.* 2016) suggesting a weaker fit between dispersal models and observed
403 genetic patterns in this region.
404
405 In summary, for the two acroporid corals considered here, we find strong support for recent
406 gene flow in a predominantly north to south direction. This result implies that northern and

407 central reefs are important sources for downstream southern reefs, at least over evolutionary
408 time scales of many generations. Downstream southern reef populations, however, harbour
409 greater genetic diversity than northern reefs and are therefore both valuable in terms of
410 distinctive diversity and likely strongly self-recruiting so that they may be more self-
411 sustaining than central and northern reefs. With temperatures and extreme heating events
412 projected to increase in frequency (Wolff *et al.* 2018), resolving the GBR-wide capacity for
413 gene flow including the directionality of naturally occurring gene flow contributes to
414 emerging debates regarding assisted migration and genetic rescue (Anthony *et al.* 2017).
415
416 *Detecting contemporary asymmetric planktonic larval dispersal*
417 Relatively few studies have evaluated the effect of asymmetric larval dispersal on spatial
418 genetic patterns in marine species (Riginos *et al.* 2016). Perhaps not surprisingly, these
419 studies, like our results here with *A. tenuis* and *A. millepora,* consistently uncover substantial
420 asymmetries in inferred dispersal (e.g. Benestan *et al.* 2016; Dalongeville *et al.* 2018; Xuereb
421 *et al.* 2018). Clearly, conventional analyses, especially those based on summary statistics like
422 F_{ST} where all directional information is obscured, will fail to uncover important elements
423 regarding relationships among populations (Kool *et al.* 2013; Riginos *et al.* 2016).
424
425 An additional challenge is to clarify the time frame for processes yielding asymmetric spatial
426 genetic patterns. Empirical genomic data paired with specific historical demographic
427 simulations can sometimes put bounds on the timing and directionality of gene flow (as in
428 Duranton *et al.* 2018; Matz *et al.* 2018), but such approaches are largely constrained to
429 examining a few populations at a time due to exponential increase in number of potential free
430 parameters (for example, if migration is free to vary among n populations then there will be
431 n!/(n-2)! parameters for directional migration). Moreover, there is greater uncertainty
432 surrounding parameter estimation for recent events (Robinson *et al.* 2014). Simple
433 frequentist approaches based on linear models such as AEMs represent an attractive
434 alternative especially as they have been conceived for uncovering contemporary structuring
435 processes in species composition of ecological communities (Dray *et al.* 2006), but if applied
436 to intraspecific genetic data these approaches are likely to be misleading when historical
437 events have strongly shaped spatial genetic patterns.
438

439 In the present study, we attempted to bridge this historical-contemporary dilemma by using
440 constrained historical demographic simulations to reject the historical scenario most likely to
441 influence observable spatial genetic patterns for GBR species, giving us greater confidence
442 that the spatial genetic patterns we observe for *A. tenuis* and (to a lesser extent) *A. millepora*
443 reflect evolutionary processes from the recent past. Using prior information based on geology,
444 historical habitat shifts, or histories of co-distributed species to identify relevant alternative
445 hypotheses and then evaluating those hypotheses against hypotheses based on contemporary
446 gene flow (such as simple stepping-stone gene flow as used here) is a reasonable check of
447 data before proceeding to interpret results from linear models (including AEMs) at face value.
448
449 *Biophysical models as summaries of larval dispersal*
450 Biophysical models are increasingly being used to make detailed spatial predictions of
451 planktonic larval dispersal often with the aim of guiding management actions (as in Hock *et al.*
452 2016; 2017; Krueck *et al.* 2017). Although such complex models of natural systems cannot be
453 truly tested (Oreskes *et al.* 1994), alignment of model outputs against independent biological
454 data can provide greater confidence that a biophysical larval dispersal model captures
455 elements of biological reality. In the present study, we find that directions and relative
456 magnitudes of dispersal connections derived from biophysical models are better predictors of
457 spatial genetic structure in *A. tenuis* and *A. millepora* than null models of symmetric
458 relationships providing a confirmation that real biological processes mirror expectations
459 arising from biophysical simulations. The superior predictive power of asymmetric predictors
460 provides further evidence of the need to consider directional flow when analysing
461 connectivity in marine systems.
462
463 For our *Acropora* species on the GBR, the strongest alignments between the models and
464 empirical genetic data are at large spatial scales (among regions) and involve north to south
465 connections. Because small numbers of migrants can homogenize allele frequencies between
466 populations, inferences based on allele frequencies are poorly suited to distinguishing
467 strengths of demographically significant connections (Waples 1998). Allele frequency based
468 methods, however, can theoretically discriminate between rare and very rare connections
469 such as those that are likely to link spatially distant populations (including via
470 multigenerational connections). Thus, the appropriate spatial scale for evaluating biophysical
471 larval dispersal models with population genetic data is at large spatial distances such a

regional connections among GBR coral populations where we find the greatest concordance between predicted and observed patterns. Comprehensive evaluation of biophysical models will best be undertaken with a variety of complementary empirical data types (Jones 2015; Gaggiotti 2017), where geographic patterns of allelic distributions contribute valuable information about rare long distance connections. Here we have shown that the directionality of such rare long distance connections discerned from spatial distributions of alleles provides additional useful information for gauging concordance of larval dispersal models against past gene flow.

ACKNOWLEDGEMENTS

We thank FG Blanchet for guidance on creating connexion diagrams and C Doropoulos for help with parameterisation of the dispersal models, the QRIS computing cluster for enabling simulation modeling, and funding support from the Great Barrier Reef Foundation.

485 **REFERENCES**

486 1.Abbey, E., Webster, J.M. & Beaman, R.J. (2011). Geomorphology of submerged reefs on the
487 shelf edge of the Great Barrier Reef: The influence of oscillating Pleistocene sea-levels. *Mar*
488 *Geol*, 288, 61–78.
489 2.Anthony, K.R.N., Bay, L., Costanza, R., Firn, J., Gunn, J., Harrison, P., *et al.* (2017). New
490 interventions are needed to save coral reefs. *Nat Ecol Evol*, 1, 1–3.
491 3.Beaumont, M.A. (2008). Joint determination of topology, divergence time, and immigration
492 in population trees. In: *Simulations, genetics and human prehistory* (eds. Matsumura, S.,
493 Forster, P. & Renfrew, C.).
494 4.Beger, M., Linke, S., Watts, M., Game, E., Treml, E.A., Ball, I., *et al.* (2010). Incorporating
495 asymmetric connectivity into spatial decision making for conservation. *Cons Lett*, 3, 359–368.
496 5.Benestan, L., Quinn, B.K., Maaroufi, H., Laporte, M., Clark, F.K., Greenwood, S.J., *et al.* (2016).
497 Seascape genomics provides evidence for thermal adaptation and current-mediated
498 population structure in American lobster (*Homarus americanus*). *Mol Ecol*, 25, 5073–5092.
499 6.Blanchet, F.G., Legendre, P. & Borcard, D. (2008). Modelling directional spatial processes in
500 ecological data. *Ecol Model*, 215, 325–336.
501 7.Blanchet, F.G., Legendre, P., Maranger, R., Monti, D. & Pepin, P. (2011). Modelling the effect of
502 directional spatial ecological processes at different scales. *Oecologia*, 166, 357–368.
503 8.Borcard, D. & Legendre, P. (2002). All-scale spatial analysis of ecological data by means of
504 principal coordinates of neighbour matrices. *Ecol Model*, 153, 51–68.
505 9.Boykov, Y. & Kolmogorov, V. (2004). An experimental comparison of min-cut/max- flow
506 algorithms for energy minimization in vision. *IEEE Trans. Pattern Anal. Machine Intell.*, 26,
507 1124–1137.
508 10.Carr, M.H., Neigel, J., Estes, J., Andelman, S., Warner, R. & Largier, J. (2003). Comparing
509 marine and terrestrial ecosystems: Implications for the design of coastal marine reserves. *Ecol*
510 *App*, 13, S90–S107.
511 11.Choukroun, S., Ridd, P.V., Brinkman, R. & McKinna, L.I.W. (2010). On the surface circulation
512 in the western Coral Sea and residence times in the Great Barrier Reef. *J Geophys Res*, 115,
513 239.
514 12.Cowen, R.K. & Sponaugle, S. (2009). Larval dispersal and marine population connectivity.
515 *Ann Rev Marine Sci*, 1, 443–466.
516 13.Crandall, E.D., Treml, E.A. & Barber, P.H. (2012). Coalescent and biophysical models of
517 stepping-stone gene flow in neritid snails. *Mol Ecol*, 21, 5579–5598.

14.Dalongeville, A., Andrello, M., Mouillot, D., Lobreaux, S., Fortin, M.-J., Lasram, F., *et al.* (2018). Geographic isolation and larval dispersal shape seascape genetic patterns differently according to spatial scale. *Evol App*, 11, 1437–1447.

15.Dijkstra, E.W. (1959). A note on two problems in connexion with graphs. *Numer. Math.*, 1, 269–271.

16.Diniz-Filho, J.A.F., Nabout, J.C., Telles, M.P. de C., Soares, T.N. & Rangel, T.F.L.V.B. (2009). A review of techniques for spatial modeling in geographical, conservation and landscape genetics. *Genet Mol Biol*, 32, 203–211.

17.Dray, S., Legendre, P. & Peres-Neto, P.R. (2006). Spatial modelling: a comprehensive framework for principal coordinate analysis of neighbour matrices (PCNM). *Ecol Model*, 196, 483–493.

18.Duranton, M., Allal, F., Fraïsse, C., Bierne, N., Bonhomme, F. & Gagnaire, P.-A. (2018). The origin and remolding of genomic islands of differentiation in the European sea bass. *Nat Comm*, 9, 1–11.

19.Excoffier, L. & Lischer, H.E.L. (2010). Arlequin suite ver 3.5: a new series of programs to perform population genetics analyses under Linux and Windows. *Mol Ecol Resour*, 10, 564–567.

20.Excoffier, L., Dupanloup, I., Huerta-Sánchez, E., Sousa, V.C. & Foll, M. (2013). Robust demographic inference from genomic and SNP data. *PLoS Genet*, 9, e1003905.

21.Ford, L.R. & Fulkerson, D.R. (1956). Maximal flow through a network. *Can J Math*, 8, 399–404.

22.Foster, N.L., Paris, C.B., Kool, J.T., Baums, I.B., Stevens, J.R., Sanchez, J.A., *et al.* (2012). Connectivity of Caribbean coral populations: complementary insights from empirical and modelled gene flow. *Mol Ecol*, 21, 1143–1157.

23.Gaggiotti, O.E. (2017). Metapopulations of Marine Species with Larval Dispersal: A Counterpoint to Ilkka's Glanville Fritillary Metapopulations. *Ann Zool Fennici*, 54, 97–112.

24.Gaines, S.D., White, C., Carr, M.H. & Palumbi, S.R. (2010). Designing marine reserve networks for both conservation and fisheries management. *Proc Natl Acad Sci USA*, 107, 18286–18293.

25.Galindo, H.M., Olson, M.V. & Palumbi, S.R. (2006). Seascape genetics: A coupled oceanographic-genetic model predicts population structure of Caribbean corals. *Curr Biol*, 16, 1622–1626.

26.Hellberg, M.E. (2009). Gene flow and isolation among populations of marine animals. *Annu*

Rev Ecol Evol Syst, 40, 291–310.
27.Hinestrosa, G., Webster, J.M. & Beaman, R.J. (2016). Postglacial sediment deposition along a mixed carbonate-siliciclastic margin: New constraints from the drowned shelf-edge reefs of the Great Barrier Reef, Australia. *Palaeogeography, Palaeoclimatology, Palaeoecology*, 446, 168–185.
28.Hock, K. & Mumby, P.J. (2015). Quantifying the reliability of dispersal paths in connectivity networks. *J R Soc Interface*, 12, 20150013–20150013.
29.Hock, K., Wolff, N.H., Beeden, R., Hoey, J., Condie, S.A., Anthony, K.R.N., *et al.* (2016). Controlling range expansion in habitat networks by adaptively targeting source populations. *Cons Biol*, 30, 856–866.
30.Hock, K., Wolff, N.H., Ortiz, J.C., Condie, S.A., Anthony, K.R.N., Blackwell, P.G., *et al.* (2017). Connectivity and systemic resilience of the Great Barrier Reef. *PLoS Biol*, 15, e2003355–23.
31.Jones, G.P. (2015). Mission impossible: unlocking the secrets of coral reef fish dispersal. In: *Ecology of Fishes on Coral Reefs* (ed. Mora, C.). Cambridge University Press, Cambridge, pp. 16–27.
32.Kool, J.T., Moilanen, A. & Treml, E.A. (2013). Population connectivity: recent advances and new perspectives. *Landscape Ecol*, 28, 165–185.
33.Kool, J.T., Paris, C.B., Andréfouët, S. & Cowen, R.K. (2010). Complex migration and the development of genetic structure in subdivided populations: an example from Caribbean coral reef ecosystems. *Ecography*, 105, 26191–10.
34.Kool, J.T., Paris, C.B., Barber, P.H. & Cowen, R.K. (2011). Connectivity and the development of population genetic structure in Indo-West Pacific coral reef communities. *Global Ecol Biogeogr*, 20, 695–706.
35.Kritzer, J.P. & Sale, P.F. (2004). Metapopulation ecology in the sea: from Levins' model to marine ecology and fisheries science. *Fish Fish*, 5, 131–140.
36.Krueck, N.C., Ahmadia, G.N., Green, A., Jones, G.P., Possingham, H.P., Riginos, C., *et al.* (2017). Incorporating larval dispersal into MPA design for both conservation and fisheries. *Ecol Appl*, 27, 925–941.
37.Liggins, L., Treml, E.A. & Riginos, C. (2013). Taking the plunge: an introduction to undertaking seascape genetic studies and using biophysical models. *Geogr Comp*, 7, 173–196.
38.Lukoschek, V., Riginos, C. & van Oppen, M.J.H. (2016). Congruent patterns of connectivity can inform management for broadcast spawning corals on the Great Barrier Reef. *Mol Ecol*, 25, 3065–3080.

584 39.Mao, Y. & Luick, J.L. (2014). Circulation in the southern Great Barrier Reef studied through
585 an integration of multiple remote sensing and in situ measurements. *J Geophys Res Oceans*,
586 119, 1621–1643.
587 40.Matz, M.V., Treml, E.A., Aglyamova, G.V. & Bay, L. (2018). Potential and limits for rapid
588 genetic adaptation to warming in a Great Barrier Reef coral. *PLoS Genet*, 14, e1007220–19.
589 41.Metaxas, A. & Saunders, M. (2009). Quantifying the "bio-" components in biophysical
590 models of larval transport in marine benthic invertebrates: advances and pitfalls. *Biol Bull*,
591 216, 257–272.
592 42.Oreskes, N., Shrader-Frechette, K. & Belitz, K. (1994). Verification, validation, and
593 confirmation of numerical models in the Earth sciences. *Science*, 263, 641–646.
594 43.Pineda, J., Hare, J.A. & Sponaugle, S. (2007). Larval transport and dispersal in the coastal
595 ocean and consequences for population connectivity. *Oceanography*, 20, 22–39.
596 44.Planes, S. & Doherty, P.J. (1997). Genetic and color interactions at a contact zone of
597 *Acanthochromis polyacanthus*: a marine fish lacking pelagic larvae. *Evolution*, 51, 1232–1243.
598 45.Pratchett, M.S., Caballes, C.F., Rivera-Posada, J.A. & Sweatman, H.P.A. (2014). Limits to
599 understanding and managing outbreaks of crown-of-thorns starfish (*Acanthaster spp*.).
600 *Oceanogr Mar Biol*, 1–68.
601 46.Pringle, J.M. & Wares, J.P. (2007). Going against the flow: maintenance of alongshore
602 variation in allele frequency in a coastal ocean. *Mar Ecol Prog Ser*, 335, 69–84.
603 47.Riginos, C. & Liggins, L. (2013). Seascape genetics: populations, individuals, and genes
604 marooned and adrift, 7, 197–216.
605 48.Riginos, C., Crandall, E.D., Liggins, L., Bongaerts, P. & Treml, E.A. (2016). Navigating the
606 currents of seascape genomics: how spatial analyses can augment population genomic
607 studies. *Curr Zool*, 62, 581–601.
608 49.Robinson, J.D., Coffman, A.J., Hickerson, M.J. & Gutenkunst, R.N. (2014). Sampling strategies
609 for frequency spectrum-based population genomic inference. *BMC Evol Biol*, 14, 254.
610 50.Roux, C., Fraïsse, C., Romiguier, J., Anciaux, Y., Galtier, N. & Bierne, N. (2016). Shedding light
611 on the grey zone of speciation along a continuum of genomic divergence. *PLoS Biol*, 14,
612 e2000234–22.
613 51.Schunter, C., Carreras-Carbonell, J., Macpherson, E., Tintoré, J., Vidal-Vijande, E., Pascual, A.,
614 *et al.* (2011). Matching genetics with oceanography: directional gene flow in a Mediterranean
615 fish species. *Mol Ecol*, 20, 5167–5181.
616 52.Selkoe, K.A., D'Aloia, C.C., Crandall, E.D., Iacchei, M., Liggins, L., Puritz, J.B., *et al.* (2016a). A

617 decade of seascape genetics: contributions to basic and applied marine connectivity. *Mar Ecol*
618 *Prog Ser*, 554, 1–19.
619 53.Selkoe, K.A., Scribner, K.T. & Galindo, H.M. (2016b). Waterscape genetics – applications of
620 landscape genetics to rivers, lakes, and seas. In: *Landscape Genetics: Concepts, Methods,*
621 *Applications* (eds. Balkenhol, N., Cushman, S.A., Storfer, A. & Waits, L.P.). John Wiley & Sons,
622 Ltd., pp. 1–27.
623 54.Sundqvist, L., Keenan, K., Zackrisson, M., Prodöhl, P. & Kleinhans, D. (2016). Directional
624 genetic differentiation and relative migration. *Ecol Evol*, 6, 3461–3475.
625 55.Thomas, L., Kennington, W.J., Stat, M., Wilkinson, S.P., Kool, J.T. & Kendrick, G.A. (2015).
626 Isolation by resistance across a complex coral reef seascape. *Proc. Biol. Sci.*, 282, 20151217.
627 56.Truelove, N.K., Kough, A.S., Behringer, D.C., Paris, C.B., Box, S.J., Preziosi, R.F., *et al.* (2016).
628 Biophysical connectivity explains population genetic structure in a highly dispersive marine
629 species. *Coral Reefs*, 1–13.
630 57.van Oppen, M.J.H., Peplow, L.M., Kinnimonth, S. & Berkelmans, R. (2011). Historical and
631 contemporary factors shape the population genetic structure of the broadcast spawning coral,
632 *Acropora millepora*, on the Great Barrier Reef. *Mol Ecol*, 20, 4899–4914.
633 58.Waples, R.S. (1998). Separating the wheat from the chaff: patterns of genetic
634 differentiation in high gene flow species. *J Hered*, 89, 438–450.
635 59.Watson, J.R., Kendall, B.E., Seigel, D.A. & Mitarai, S. (2012). Changing seascapes, stochastic
636 connectivity, and marine metapopulation dynamics. *Am. Nat.*, 180, 99–112.
637 60.Werner, F. & Cowen, R.K. (2007). Coupled biological and physical models: present
638 capabilities and necessary developments for future studies of population connectivity.
639 *Oceanography*, 20, 54–69.
640 61.White, C., Selkoe, K.A., Watson, J., Siegel, D.A., Zacherl, D.C. & Toonen, R.J. (2010). Ocean
641 currents help explain population genetic structure. *Proc. Biol. Sci.*, 277, 1685–1694.
642 62.Whitlock, M.C. & McCauley, D.E. (1999). Indirect measures of gene flow and migration: FST
643 not equal to 1/(4Nm + 1). *Heredity*, 82, 117–125.
644 63.Wolff, N.H., Mumby, P.J., Devlin, M. & Anthony, K.R.N. (2018). Vulnerability of the Great
645 Barrier Reef to climate change and local pressures. *Global Change Biol*, 24, 1978–1991.
646 64.Xuereb, A., Benestan, L., Normandeau, E., Curtis, J.M., Bernatchez, L. & Fortin, M.-J. (2018).
647 Asymmetric oceanographic processes mediate connectivity and population genetic structure,
648 as revealed by RADseq, in a highly dispersive marine invertebrate (*Parastichopus*
649 *californicus*). *Mol Ecol*, 1–46.

TABLES

Table 1: Spatial eigenvector map modelling of genetic structure. The models explaining the greatest amount of genetic variance are those that incorporate directional link structures derived from the larval dispersal model, especially those that are based on north to south alongshore flow.

		Acropora tenuis			*Acropora millepora*		
Eigenmodel	**Link structure**	**Link weighting of best model** [a]	**Numb EMs in best model** [b]	**adjusted R^2** [b]	**Link weighting of best model** [a]	**Numb EMs in best model** [b]	**adjusted R^2** [b]
MEM	Delauney	Binary	1	0.02	Binary	1	0.02
MEM	Delauney	log	1	0.04	log	1	0.04
MEM	PCNM	y=1	**4**	**0.24**	y=1	**1**	**0.09**
MEM	Custom saturated	y=1	3	0.16	y=1	1	0.07
AEM	Alongshore N to S only [c]	MF, y=1	**9**	**0.37**	Binary	**5**	**0.27**
AEM	Alongshore both N to S and S to N	SS, y=1	8	0.29	MF, y=1	2	0.15

[a] Binary distances represent a single model. The link structures were evaluated for link distance weightings based on the formula $1-(D/Dmax)^y$ for y=[1-3] or with a log transformation to approximate a typical isolation-by-distance analysis. For AEMs, links were limited to those in the top 50 percentile of reliable path weights. Link weightings were evaluated based on the number of stepping stone (SS) connections, maximum flow (MF), and reliable path (RP) strength.

[b] Following forward model selection.

[c] Select AEMs shown graphically in Fig. 3 and Sup. Fig. 2

Table 2: Asymmetric eigenvector map modelling regions within *Acropora tenuis*

	Best model by region			
Region	**Link structure**	**Link weighting** [a]	**Numb EMs in best model** [b]	**adjusted R^2** [b]
Far north & north	Alongshore both N to S and S to N	MF, y=1	**3**	0.17
North, central, south	Alongshore N to S	MF, y=1	**7**	0.32
Central & south	Alongshore N to S	RP, y=2	**5**	0.35

[a] Link structures were evaluated for distance weightings based on the formula $1-(D/Dmax)^y$ for y=[1-3].

[b] Following forward model selection.

667 **FIGURE LEGENDS**

668 **Figure 1:** Sampling locations and main attributes of biophysical model. A) Coastal Queensland
669 and the Great Barrier Reef where bathymetry is shown by grey shading and 120 m depth
670 reflects the approximate land mass exposure at lowest Pleistocene sea level stands.
671 Designated regions correspond to management areas. Major offshore currents are shown
672 (NVJ and SVJ: north and south Vanuatu jets, NQC: north Queensland current, EAC: east
673 Australia current; modified from Coukroun *et al.* 2010; Mao & Luick 2014). B & C) Summary of
674 top 50 percentile predicted connections based on relative path probabilities for *Acropora*
675 *tenuis* (B) and *Acropora millepora* (C). Sampling locations are color coded by latitude with
676 northern low latitude sites shown in reds (warm) and southern higher latitude sites shown in
677 blues (cool). Vectors show predicted dispersal probabilities with thicker lines indicating
678 higher probabilities and colored by source population. D & E) Dispersal probabilities relative
679 to coastline position for *Acropora tenuis* (D) and *Acropora millepora* (E). The largest positional
680 changes northwards have the lowest probabilities whereas small positional changes and
681 movements southwards have higher probabilities. Movement relative to coastline is based on
682 the difference in relative position between locations as summarised by the first principal
683 component axis describing Queensland coastline. Example contrasts in northward vs.
684 southward dispersal strengths shown for example population pairs (a,b and c,d) traversing
685 the length of the sampling region where a->b and c->d are high probabilities ($P \approx 10^{-20}$) of
686 southward movement (-4 relative positional change) and b->a and d->c are low probabilities
687 ($P \approx 10^{-40}$) of northward movement (+4 relative positional change).

688

689 **Figure 2:** Concordance in directional movement between the larval dispersal model and
690 genetic estimates for pairs of populations for *Acropora tenuis* (A), and *Acropora millepora* (B).
691 Routes of low predicted connectivity (small relative path probabilities: $P < 10^{-40}$) experience
692 low directional gene flow (using the DivMigrate method). Routes of high predicted
693 connectivity ($P > 10^{-20}$) have variable rates of gene flow.

694

695 **Figure 3:** Leading asymmetric eigenvector maps describing spatial genetic structure in
696 *Acropora tenuis*. Values by sampling location are colored by intensity of green hue such that
697 locations with similar colors have similar AEM values. The greatest proportion of variance
698 (AEM 1) describes a GBR-wide cline in genetic diversity followed by local scale spatial
699 autocorrelation structures (AEM 5).

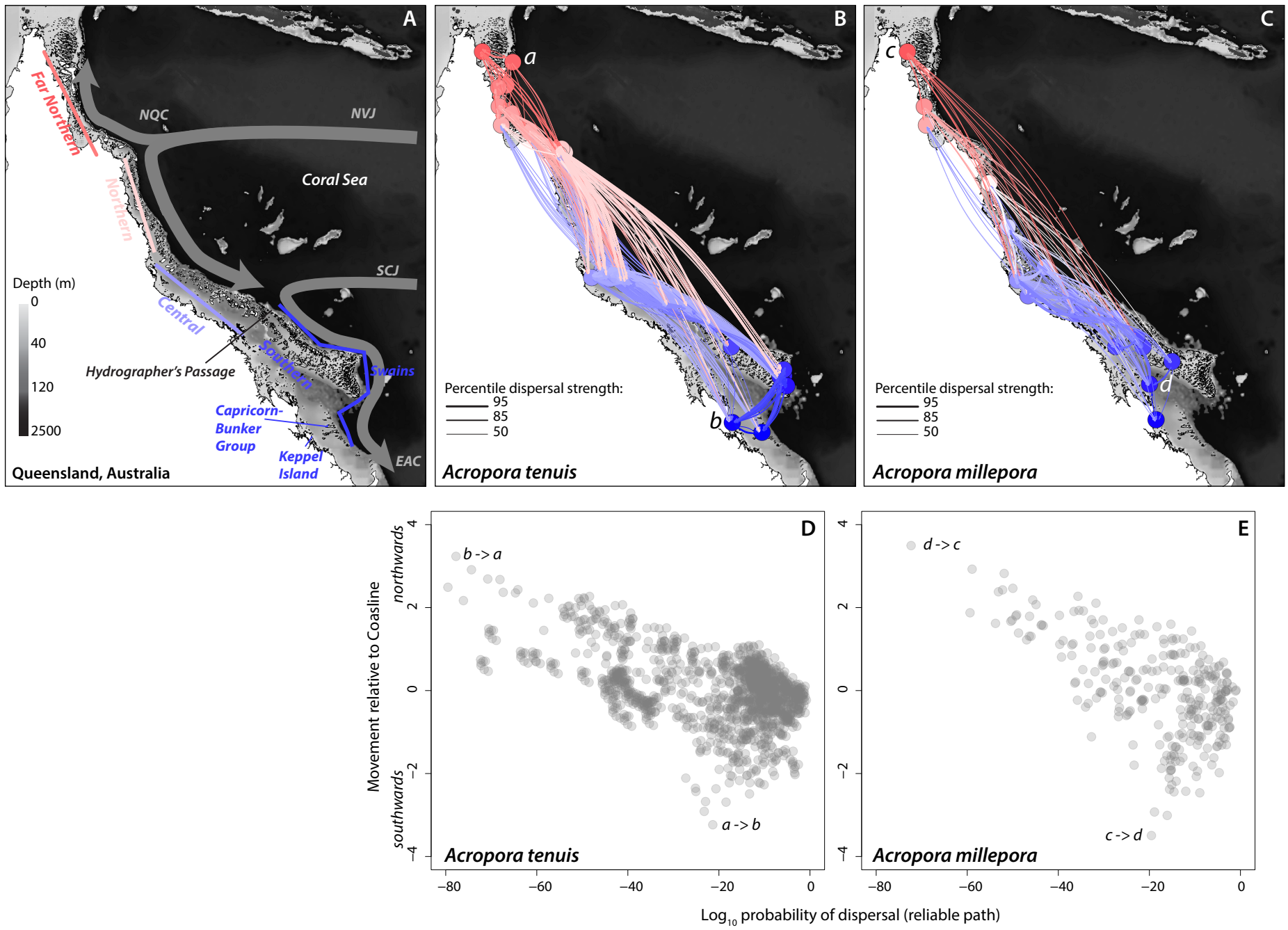
A
Far Northern
Northern
Central
Southern
NQC
NVJ
Coral Sea
SCJ
Swains
EAC
Depth (m)
0
40
120
2500
Hydrographer's Passage
Capricorn-Bunker Group
Keppel Island
Queensland, Australia
B
a
b
Percentile dispersal strength:
95
85
50
Acropora tenuis
C
c
d
Percentile dispersal strength:
95
85
50
Acropora millepora
D
b -> a
a -> b
Acropora tenuis
E
d -> c
c -> d
Acropora millepora
Movement relative to Coasline
northwards
southwards
4
2
0
−2
−4
−80
−60
−40
−20
0
Log10 probability of dispersal (reliable path)

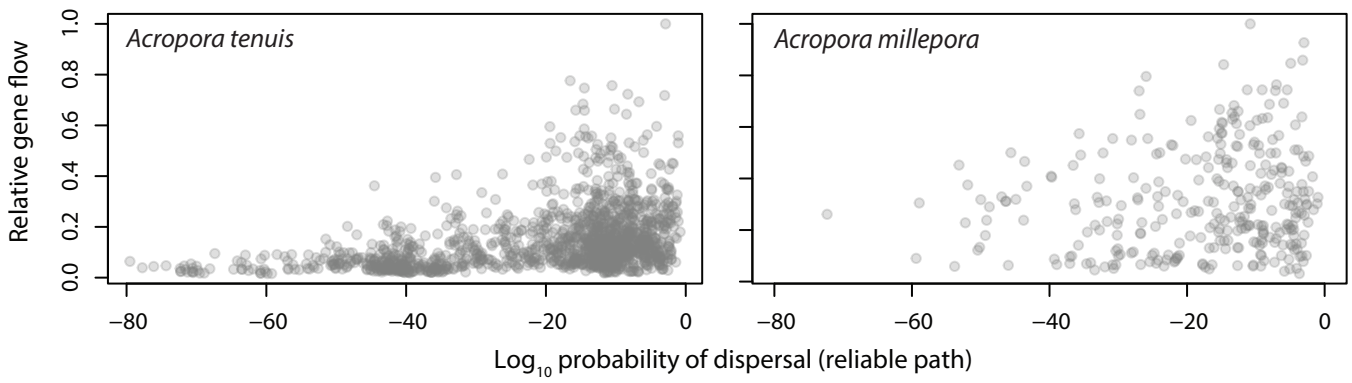
Acropora tenuis
Acropora millepora
Relative gene flow
0.0
0.2
0.4
0.6
0.8
1.0
−80
−60
−40
−20
0
Log10 probability of dispersal (reliable path)

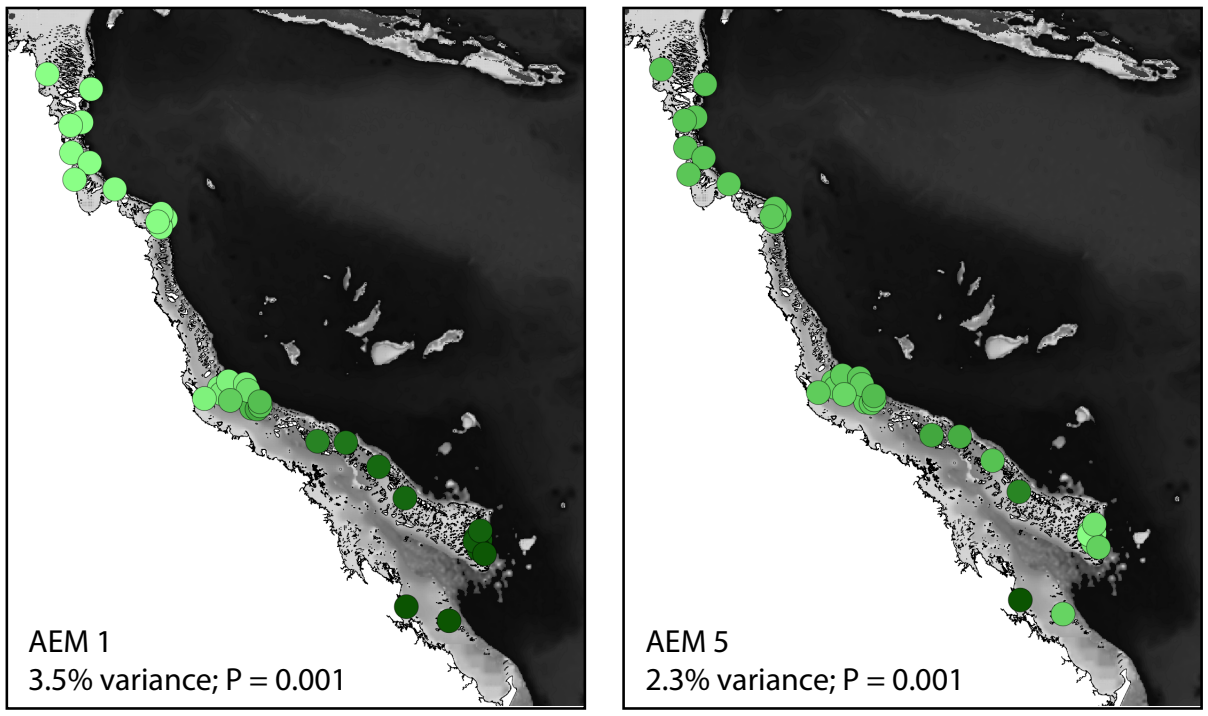
AEM 1
3.5% variance; P = 0.001
AEM 5
2.3% variance; P = 0.001